MONTE CARLO METHODS FOR VISUALIZING UNCERTAINTY ON TERNARY PLOTS WITH CHEMCAM AND SUPERCAM DATA. A. Essunfeld (aessunfeld@lanl.gov)[1], J. M. Comellas[1,2], P. J. Gasda[1], C. Legett[1], N. Lanza[1], D. Delapp[1], S. Clegg[1], R. Wiens[3], S. Maurice[4], R. Anderson[5]; [1]Los Alamos National Laboratory, [2]University of Hawai'i at Mānoa, [3]Purdue University, [4]IRAP, Toulouse, France, [5]USGS.

Introduction: NASA's *Curiosity* and *Perseverance* rovers are traversing Mars' Gale and Jezero craters, respectively [1-3]. Each rover is equipped with a chemistry camera instrument (ChemCam and SuperCam, respectively) capable of providing chemical composition data for rock targets on the surface of Mars [2-5]. The data from these instruments is often plotted on ternary diagrams to aid in mineralogical classification and to compare new observations with previous trends [e.g., 6-9]. However, it can be difficult to visualize uncertainty on ternary diagrams, and without a clear depiction of the uncertainty associated with specific datapoints, it can be hard to make mineralogical distinctions with measurable confidence.

Other methods [e.g., 10] determine ternary diagram error bars analytically and display these at fixed, representative locations on the plot. In this work, we present a new tool which leverages Monte Carlo methods to simulate data for any small set of datapoints, then uses that simulated data to compute and plot confidence regions around each point. This tool was built for both ChemCam and SuperCam data, but it could be applied to any geochemical dataset to provide users with a simple solution for finding and plotting confidence regions around their data on ternary diagrams.

Methods: Curiosity's ChemCam instrument and Perseverance's SuperCam instrument are both laser-induced breakdown spectroscopy (LIBS) instruments that provide chemical composition data of each observation point on a rock target [2-5]. LIBS data for an observation point contains predictions and associated prediction accuracies for eight major oxides, given in weight percent (wt%) [2-5]. To use this tool, a user provides a compositions file with a small number of datapoints. The tool's configuration file is used to pick which oxides should appear on the vertices of the ternary diagram, and to set other parameters, such as how many points to simulate (n) per datapoint provided. For each datapoint, the predicted value of each oxide p_{oxide} and the associated accuracy of that prediction d_{oxide} are used to create a random normal distribution of size n centered at p_{oxide} with standard deviation d_{oxide}. This is done with the `random.normal` method from the python library `numpy` [11].

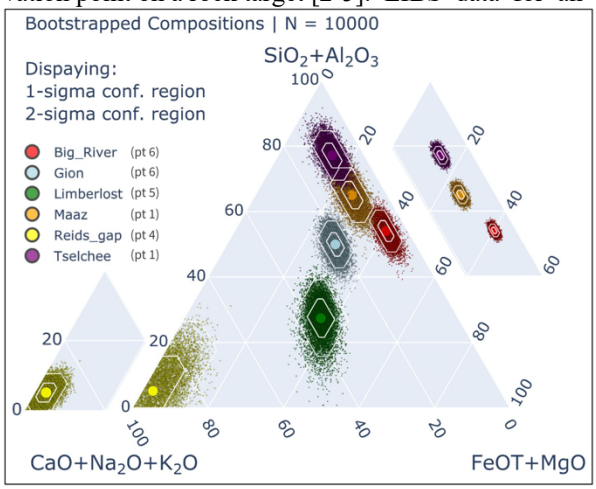

Fig. 1: SiO_2+Al_2O_3 | CaO+Na_2O+K_2O | FeO_T+MgO ternary diagram showing bootstrapped compositions and confidence regions for observation points from six SuperCam Mars rock targets. Model accuracy [see 12] is used for bootstrapping on the center ternary; results obtained using instrument precision [see 12] are shown in cutouts on the upper right and lower left for comparison.

This process extends the provided dataset by a factor of $n \cdot k$, where k is the number of datapoints provided. Molar proportion (hereafter "molar") data is then calculated from the simulated wt% data as follows: First, the values of the oxides being used in the ternary diagram are normalized using the sum of the point's composition values across just those oxides. Next, those values are converted from wt% to molar by dividing each normalized wt% value by the corresponding oxide's molar mass. This molar data is then renormalized using the sum of the molar values. The appropriate molar proportions are then summed in accordance with the formulae provided for each vertex of the ternary diagram. This process further extends the dataset with three new columns: one for the molar proportion of each vertex (V_1, V_2, and V_3).

To plot the confidence regions around each datapoint, the median and standard deviation of that point's simulated data is calculated and stored as m_i and d_i, respectively, for each vertex column V_i. Parallel lines are then drawn at the 1- and 2-sigma distances above and below the median of the distribution, perpendicular to the corresponding axes of the ternary. The region enclosed by these three pairs of parallel lines (often hexagonal, sometimes parallelogrammatic) is then displayed as an approximation for the corresponding confidence region. Once this process is complete, the resulting figure and simulated data are saved.

Results: The tool itself provides a flexible and easy-to-use solution for creating ternary diagrams with approximate uncertainty quantification. The plots created by the tool display the datapoints provided by the user ("anchor points") as large circles, the simulated data as a cloud of points around each anchor point, and (if the user specifies) the crosshatches and confidence regions corresponding to 1- and 2-sigma for each point cloud. Different anchor points are displayed with different colors. The uncertainty quantification features being displayed are listed in the upper left legend. The

title of each plot contains the value of *n*, the number of simulated points per anchor point.

Figure 1 is a ternary diagram generated by this tool showing bootstrapped composition data and 1- and 2-sigma confidence regions for six different SuperCam observation points. These points represent three early-mission Mars rock targets (*Máaz*, *Tselchee*, and *Big_River*), along with three targets chosen for their varying elevated CaO (*Gion* pt. 6: 19 wt%; *Limberlost* pt. 5: 27 wt%; *Reids_gap* pt. 4: 50 wt%). For this plot, we used $n = 10^4$. The points provided to simulate data are plotted as large circles at the center of each point cloud, and the simulated points are plotted as much smaller circles. The formulae used for each vertex of the ternary are shown at the vertices of the plot.

Figure 2 is another ternary diagram generated by this tool showing bootstrapped composition data and 1- and 2-sigma confidence regions for four different ChemCam observation points. The points from *Angmaat* and *Kukri* plot near the SA vertex, as they are comprised mostly of silica and aluminum. The point from *Harrison* plots closer to the FM vertex, having unusually high iron. And the point from *Rapitan* plots very near the CNK vertex, with a noticeably larger confidence region compared to the other three points.

Discussion: Typically, points near the CNK vertex (or more specifically, points with high CaO values) will have lower major oxide composition totals. Because of this, and the renormalization involved in finding molar proportions, the uncertainty for the CaO prediction has more sway over the entire distribution than the uncertainty on, for instance, the SiO_2 prediction. The result is the trend seen in both Figures 1 and 2, whether using accuracy or precision: points near the CNK vertex exhibit significantly larger confidence regions than points near the SA vertex. This supports the argument that the uncertainty of a specific point on a ternary diagram will depend on its underlying composition and its location on the plot.

In Figure 1, the 2-sigma confidence regions of *Tselchee* and *Máaz* overlap, while the 1-sigma confidence regions are disjoint. When instrument precision [see 12] is used to bootstrap, rather than model accuracy [see 12-14], their entire distributions are disjoint (Fig. 1, upper right). When ternary diagrams are used to aid in geochemical classification, bootstrapping, as done with this tool, can be helpful in determining how likely it is that a target belongs to a given endmember. Additionally, if the points being used as representatives for different endmembers overlap significantly in their confidence regions even when bootstrapped using precision, the ability to visualize that can help motivate development for improved calibrations. Worth noting is that the current SuperCam prediction uncertainties are provisional, and an improved calibration is being actively worked. Additionally, the use of a Gaussian to simulate data is an assumption that only approximates the true distribution, and it may result in wider spread.

In developing this tool, we wrote three Python classes: a `Ternary` class, with methods for plotting and saving ternaries; a `LIBSData` class for representing

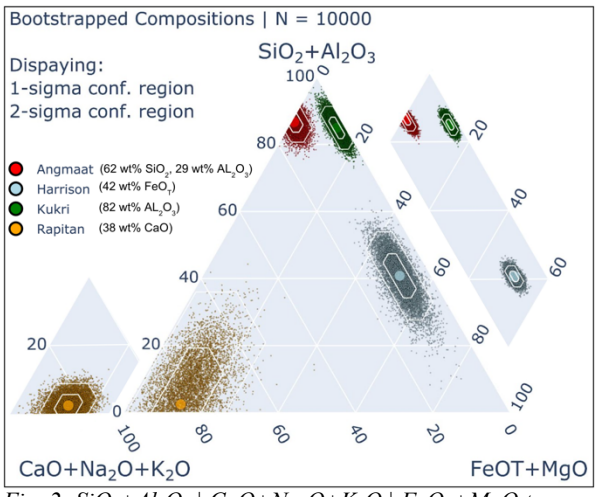

Fig. 2: SiO_2+Al_2O_3 | CaO+Na_2O+K_2O | FeO_T+MgO ternary diagram showing bootstrapped compositions and confidence regions for observation points from four ChemCam targets: Angmaat, Harrison, Kukri, and Rapitan. Model accuracy [13-14] is used for bootstrapping on the center ternary; results obtained using instrument precision [13-14] are shown in cutouts on the upper right and lower left for comparison.

generic LIBS data (compatible with both ChemCam and SuperCam data), with methods for bootstrapping and saving simulated data, and a `Config` class for representing configuration files, a common feature of team-built tools for processing LIBS data. We hope to make the code base accessible to facilitate future tool development involving geochemical data and ternary diagram generation.

Conclusion & Future Work: Bootstrapping provides an effective means for displaying approximate LIBS data uncertainty on ternary diagrams. Visualizing confidence regions this way is dynamic with the position of a point on the diagram, helps in geochemical classification, and motivates further calibration development. Going forward, we hope to develop a refined method for plotting confidence regions that captures their true ellipsoidal shape better than the current hexagonal approximations. We will also explore the use of other non-normal distributions in bootstrapping to attempt to better capture the true data distribution.

Acknowledgements: NASA Mars Exploration Program, JPL, CNES.

References: [1] Grotzinger J et al. (2014) *Science, 343(6169).* [2] Maurice S et al. (2021) *Space Sci Rev, 217, 47.* [3] Wiens RC et al. (2021) *Space Sci Rev, 217, 4.* [4] Wiens RC et al. (2012) *SSR, 170:167–227.* [5] Maurice S et al. (2012) *SSR, 170:95-166.* [6] Hurowitz JA et al. (2006) *JGR, 111, E02S19.* [7] Comellas JM et al. (2021) *52nd LPSC Abstract #2176.* [8] Comellas JM et al. (2022) *53rd LPSC Abstract #2445.* [9] Gasda PJ et al. (2022) *53rd LPSC Abstract #1654.* [10] Wiens RC et al. (2022) *Sci. Adv. 8.* [11] Harris CR et al. (2020) *Nature 585, 357–362.* [12] Anderson RB et al. (2022) *Spectrochimica Acta Pt. B: Atomic Spectroscopy 188:106347.* [13] Clegg SM et al. (2017) *Spectrochimica Acta Pt. B: Atomic Spectroscopy* 129:64–85. [14] Blaney DL et al. (2014) *JGR Planets 119:2109–2131.*